# Fast Shielding Optimization of an Inductive Power Transfer System for Electric Vehicles

Yao Pei, Lionel Pichon, Yann Le Bihan, Mohamed Bensetti, Philippe Dessante

IEEE Access
Multidisciplinary | Rapid Review | Open Access Journal

Received 13 July 2022, accepted 9 August 2022, date of publication 16 August 2022, date of current version 2 September 2022.

*Digital Object Identifier 10.1109/ACCESS.2022.3198953*

RESEARCH ARTICLE

# Fast Shielding Optimization of an Inductive Power Transfer System for Electric Vehicles

**YAO PEI, LIONEL PICHON, YANN LE BIHAN, MOHAMED BENSETTI, AND PHILIPPE DESSANTE**

Laboratoire de Génie Electrique et Electronique de Paris, CentraleSupélec, CNRS, Université Paris-Saclay, 91192 Gif-sur-Yvette, France
Laboratoire de Génie Electriqueet Electronique de Paris, CNRS, Sorbonne Université, 75252 Paris, France

Corresponding author: Yao Pei (yao.pei@centralesupelec.fr)

**ABSTRACT** The shielding design is one of the most difficult phases in developing an inductive power transfer system (IPT) for electric vehicles. In this aspect, the combination of metamodeling with a multiobjective optimization algorithm provides an efficient approach. Here, Polynomial Chaos Expansions (PCE) and Multigene Genetic Programming Algorithm (MGPA) methods are used and compared to describe the mutual inductance of the IPT system in the function of the design variables on the shielding. These metamodels are obtained based on a number of 3D Finite Element Method (FEM) computations. Then, a multiobjective optimization algorithm coupled with the PCE metamodeling technique is applied to determine the optimal design variables for a practical shielding design when considering the magnetic coupling as well as the cost of the shielding as objective functions. Such a multiobjective optimization algorithm based on a particle swarm algorithm coupled with a metamodel on PCE method is proposed, leading to improve around 104 % of the mutual inductance $M$ and save 14 % of the cost $C$ for the shielding compared to the initial design.

**INDEX TERMS** Shielding design, polynomial chaos expansion, multigene genetic programming algorithm, particle swarm algorithm, inductive power transfer system.

## I. INTRODUCTION

An inductive power transfer (IPT) system for recharging electric vehicles (EV) is a technology that avoids electrical or mechanical contact. Galvanic isolation and spark-free operation of the IPT system will further enhance the safety aspects of charging EVs. It allows both stationary and dynamic charging [1].

In general, the IPT system uses a transmitter and a receiver where ferrite cores improve power transfer and work as magnetic shielding. At the same time, the EV's chassis plate also acts as shielding. It is generally made of two kinds of material respectively: the first is steel material. In a frequency operated in an EV charging IPT system, the chassis causes eddy current losses in the magnetic field generated by the transmitting coil. Even if a ferrite is installed, there is still a strong magnetic flux leakage outside the ferrite core plate [2]; the other is carbon-fiber laminate (CF). Compared to the steel plate, carbon fibers are slightly stiffer. Nowadays, carbon fiber production is expensive, so carbon-laminate composites are only used in structures that are entirely performance-oriented. However, the shielding performances of the CF composite panels are very poor [3]. Therefore, relying only on the ferrite plate to shield the magnetic flux leakage is not only expensive but also often ineffective and heavy for the receiver installed on the electric vehicles. So an aluminum plate between the chassis and the ferrite for the receiver is required to keep the transmission efficiency, minimize the cost of the shielding design and mitigate the magnetic field formed by the IPT transmitting coil. The optimization of such shielding in practical 3D configurations remains a key point in the design of efficient IPT systems.

To meet the design aims above, multiobjective optimization algorithms have been widely used in the IPT system domain, such as the Non-dominated Sorting Genetic Algorithm II (NSGA-II) [4] and multiobjective particle swarm (MOPSO) algorithm [5]. Reference [6], [7], [8], [9], [10], [11], [12], [13], [14], [15], [16] used the multiobjective optimization algorithms with 3D FEMs to analyze the performance of IPT systems. A comprehensive parametric sweep can be time-consuming, depending on the number of variables and the parameters defined for the optimization

The associate editor coordinating the review of this manuscript and approving it for publication was Agustin Leobardo Herrera-May.

algorithms. So some researchers proposed some approaches: one is to run sweeps of only significant parameters that impact the system performance [6], [7], [8], [9], [10], and the other is to select a base pad design and then sweep the selected critical parameters [11], [12], [13], [14], [15], [16] separately. These research papers did not mention the exact computational time spent in the whole process (3D FEM with the optimization algorithms).

To strongly reduce the time cost of such multiobjective optimization with 3D FEM computations, the relationship between observed outputs (mutual inductance, coupling coefficient, leakage field flux density, coil quality factor, and so on) and design variables (coils and ferrite shape, size, thickness, material properties) has been explored recently by several metamodeling techniques. In [17], [18], and [19], the authors proposed the multiobjective GPA (MGPA) method to express the self-inductance and the mutual inductance versus geometrical parameters of the ferrite and coils, which needs nearly 1000 samples (five variables) to find an accurate behavior model. References [20], [21] introduced a polynomial chaos expansion method to build a metamodel to express the mutual inductance in the case of different situations covering a wide range of geometrical parameters and material properties, which demanded small data set (55 samples for four variables). These approaches allow obtaining the performances of the system and may be very useful for a sensitivity analysis. Nevertheless, they have never been combined with an optimization algorithm for the analysis of the IPT system. Optimizing a realistic/practical problem with a traditional approach (coupling, for example, 3D FEM with an optimization algorithm) is very costly. Instead, using a metamodel with an optimization algorithm drastically reduces the computational time.

The aim of this paper is to prove that the multiobjective optimization methods can be used very efficiently with the PCE metamodeling to find the best shielding dimensions of the system, taking into account both the transmission efficiency and the cost. This approach is applied to a practical IPT system under perfect alignment conditions. Section II analyzes the relationship between the maximum transmission efficiency and the mutual inductance and discusses how FEM calculations work on the 3D structure. Section III introduces the Polynomial Chaos Expansions (PCE) method and MGPA method to build metamodels for quantifying how the mutual inductance is influenced by the geometrical dimensions of the shielding based on the training data set from 3D FEM computations. Section IV is devoted to the combination of the PCE metamodeling technique with different multiobjective algorithms. Conclusions are drawn in Section V.

## II. PROBLEM STATEMENT

The design of an IPT system involves system-level specifications that must be matched with a proper choice of architectures and components. These requirements include system performances (efficiency, voltage, current), budgets (cost, volume), environmental conditions, and system reliability (robustness, lifetime). Fig.1 shows the block diagram of an IPT system. The operating parameters of the system considered in this paper are listed in Table 1 [22], [23].

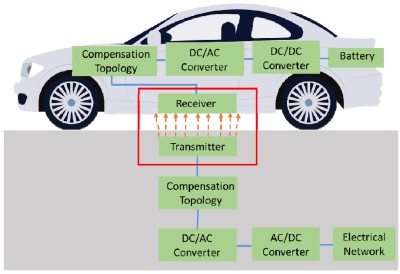


**FIGURE 1.** An inductive power transfer system.

**TABLE 1.** Simulation parameters and IPT operating status.

| Parameter | Value | Unit |
|---|---|---|
| Operating frequency $f_0$ | 85 | kHz |
| Transmitter power | 2500 | W |
| Transmitting coil current | 42 | A |
| Air gap | 150 | mm |

In this work, as shown in Fig. 2, the IPT system is a realistic 3D structure consisting of two identical rectangle-shaped coils with copper windings (orange), ferrite core plates (dark grey) [23], and aluminum plate (blue) [22]. Here, the ferrite and aluminum plates are collectively referred to form the shielding. The dimensions of the IPT system are shown in Table 2. The turns of the coils were predefined because they corresponded to an existing system for power transfer that was built and studied in GeePs (See references [22], [23]), and the external size of the coils was predefined because references [24], [25] provided some design guidelines that the optimal value of the width of a rectangular coil is three times the air gap between the transmitter and the receiver.

For the IPT system transmission efficiency, circuit models with lumped parameters are often used, and the compensation networks are designed to minimize the reactive component of the power supply. Following [1], [20], [22], [23], the series-series compensation is taken into account. Equation (1) describes the relationship between the maximum transmission efficiency $\eta_{\max}$ and the mutual inductance $M$ when the transmitter and the receiver are identical [20].

$$\eta_{\max} = 1 - \frac{R_1}{\pi f_0 M} \tag{1}$$

where $R_1$ is the resistance of the transmitter as same as the receiver.

The mutual inductance $M$ is mainly influenced by the air gap between the transmitter and the receiver indicated in the red frame in Fig.1. According to the system power, the size and shape of the coils have been previously defined [22], [23], but how to define the shielding (ferrite and aluminum) remains a challenging problem for the global system efficiency and the total cost.

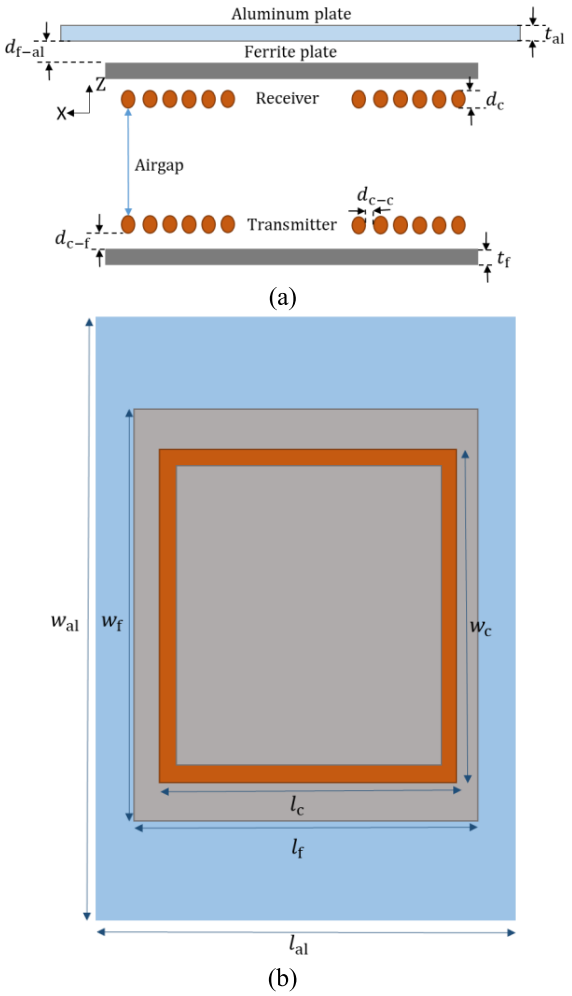


**FIGURE 2.** (a) A pair of coils (orange) with ferrite plate (grey) and aluminum plate (blue) and (b) a single rectangular coil with shielding plates.

Here, a full 3D numerical model of the IPT system has been implemented in the commercial software COMSOL [26]. The coil windings are modeled as homogenous volumes with a uniform current density [18]. Preliminary studies [1], [18] have shown that this assumption has a negligible impact on the final value of the observables (mutual inductance and magnetic field). Then, a second-order Artificial Material Single Layer Method (AMSL) [27] was adopted for the modeling of aluminum shielding instead of transition boundary condition in order to save computational time. The global mesh leads to 712225 elements. The time for a single 3D FEM computation was about 4∼5 minutes on an Intel Xeon W-2125 processor, but when calculating the mutual inductance $M$ with the metamodel, it needs less than 1 second.

In order to save the computational time for the whole optimization process, the design process of the IPT system consists of two parts: a metamodel to describe the mutual inductance $M$ dependence with the design variables (in the red line framework) instead of 3D FEM computations (in the black dotted line framework), and an algorithm to perform the optimization, as shown in Fig.3.

**TABLE 2.** Parameters of the IPT system.

| Symbol | Quantity | Value [Unit] |
|---|---|---|
| $l_c$ | External length dimension of the coils | 450 [mm] |
| $w_c$ | External width dimension of the coils | 486 [mm] |
| $d_c$ | Coil thickness | 5 [mm] |
| $d_{c\text{-}c}$ | Distance between wire and wire | 0.3 [mm] |
| $l_f$ | Ferrite length | 500 [mm] |
| $w_f$ | Ferrite width | 600 [mm] |
| $d_{c\text{-}f}$ | Distance between coil and ferrite | 8 [mm] |
| $t_f$ | Ferrite thickness | 2 [mm] |
| $l_{al}$ | Aluminum length | 800 [mm] |
| $w_{al}$ | Aluminum width | 1800 [mm] |
| $t_{al}$ | Aluminum thickness | 2 [mm] |
| $d_{f\text{-}al}$ | Distance between ferrite and aluminum | 5 [mm] |
| $\mu_r$ | Ferrite relative permeability | 3000 |
| $\sigma_{al}$ | Aluminum conductivity | 34.2 [MS/m] |
| $N$ | Coil turns | 6 |

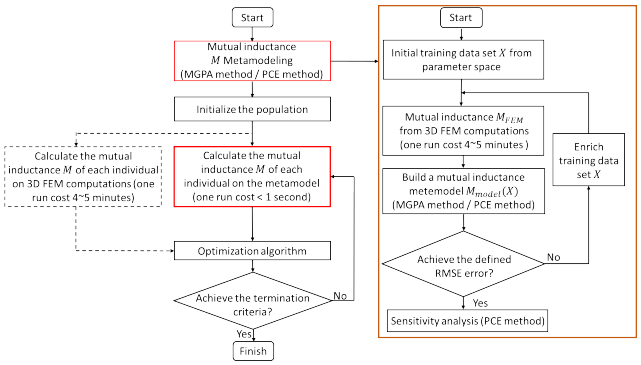


**FIGURE 3.** General flowchart of the design process.

## III. MUTUAL INDUCTANCE METAMODELING

Now, PCE [28] and MGPA [29] methods are investigated to describe how the mutual inductance $M$ (unit: $\mu H$) is influenced by the properties of the shielding. The procedure to identify these metamodels is shown in the orange line framework in Fig.3. Given the geometry and the ranges of possible geometrical dimensions of the shielding, the design can be achieved by working on the following eight design variables given in Table 3 with their range of value:

### A. MUTUAL INDUCTANCE METAMODEL ON PCE METHOD

The metamodel for expressing the mutual inductance $M$ based on a vector $\boldsymbol{X}$ of $N$ independent design variables is shown based on the PCE method:

$$\hat{M} = \sum_{\alpha \in A} c_\alpha \Phi_\alpha(X) \tag{2}$$

where $\Phi_\alpha(\boldsymbol{X})$ are multivariate polynomials orthonormal with respect to the joint probability density function of the design

**TABLE 3.** Range of the shielding geometrical dimensions.

| Parameter | Min [mm] | Max [mm] |
|---|---|---|
| $d_{\text{c-c}}$ | 1 | 5 |
| $w_{\text{f}}$ | 536 | 974 |
| $l_{\text{f}}$ | 495 | 900 |
| $d_{\text{c-f}}$ | 1 | 10 |
| $t_{\text{f}}$ | 1 | 10 |
| $w_{\text{al}}$ | 590 | 1072 |
| $l_{\text{al}}$ | 545 | 990 |
| $d_{\text{f-al}}$ | 1 | 20 |

variables $x_1, \cdots, x_N$. Here, all the design variables follow a uniform distribution, so the orthogonal polynomials are Legendre. In (2) $\alpha$ is a multi-index that identifies the components of the multivariate polynomials $\Phi_\alpha(\boldsymbol{X})$ [28]; $A$ is the set of selected multi-indices of multivariate polynomials. The hyperbolic truncation scheme makes use of the so-called $q-$norm to define the truncation, and it consists in retaining all multi-indices $\alpha$ of $q-$norm $(0 < q \leq 1)$ less than or equal to the degree $p$ as follows [28]:

$$A^{N,p,q} = \{\alpha \in \mathbb{N}^N : \|\alpha\|_q = \left(\sum_{i=1}^{N} \alpha_i^q\right)^{1/q} \leq p\} \tag{3}$$

In order to reduce the number of samples to build an accurate metamodel on the PCE method, the Least Angle Regression (LAR) is adapted to decrease the number of coefficients with high-dimensional problems to be estimated in PCE. It allows selecting the polynomial bases which have the most effect on $\hat{M}$ the truncation set $A^{N,p,q}$. For more details, readers may refer to [28], [30].

Then, based on the PCE metamodel, a sensitivity analysis can be easily performed with the coefficients of this metamodel. The first-order PCE-based Sobol index $S_i$ for the input design variable $x_i$ can be estimated as [31]:

$$S_i = \frac{Var_{\mathbf{X}_i}[E_{\mathbf{X}_{\sim i}}[\hat{M}(X)|x_i]]}{V[\hat{M}(X)]} = \frac{\sum\limits_{\alpha \in A_i} c_\alpha^2}{\sum\limits_{\alpha \in A \setminus \{0\}} c_\alpha^2} \tag{4}$$

with $A_i = \{\alpha \in A : \alpha_i > 0, \alpha_j = 0, \forall j \neq i\}$ and $\boldsymbol{X}_{\sim i}$ notation indicates the set of all variables except $x_i$. The $S_i$ of the $i^{th}$ variable closer to 1 shows that this variable has more impact on the mutual inductance $M$.

In a word, the advantage of the PCE method is that it needs a smaller number of training samples to achieve accurate results when using the LAR method compared to the traditional models. Another strong advantage, as described above, is to easily perform a sensitivity analysis to determine the most impacting parameter, since the Sobol's indices can be directly expressed with the coefficients of the polynomials.

In this paper, the sparse PCE metamodels are constructed with an adaptive degree varying from 5 to 20, and the hyperbolic scheme in Equation (3) is set to $q = 0.45$ reduce the size of the polynomial basis.

### B. MUTUAL INDUCTANCE METAMODEL ON MGPA METHOD

In MGPA, each prediction $\breve{M}$ of the mutual inductance $M$ is formed by the weighted output of each of the genes in the multigene individual plus a bias term. Each gene is a function of the $N$ input variables $x_1, \cdots, x_N$. The mutual inductance metamodel $\breve{M}$ on the MGPA method can be written as [29]:

$$\breve{M} = d_0 + d_1 \times gene1 + \cdots + d_Q \times geneQ \tag{5}$$

where $d_0$ = bias term; $d_1, \cdots, d_Q$ are the gene weights; $Q$ is the number of genes. The weights are automatically determined by a least-square procedure for each multigene individual. The number and structure of the genes may include a set of elementary functions (sum, multiplication, division, logarithm, arctangent, hyperbolic tangent, sine, exponential, and power function, etc.), which is automatically evolved during a run using training data set [17], [18], [29].

The process to build the mutual inductance metamodel on the MGPA method is [17], [18], [29]: MGPA works on a population of individuals (models), each one representing a potential solution for the mutual inductance. During its evolution, the MGPA transforms the current population of models into a new population by applying the classical genetic operations (selections, cross-over, mutation, etc.). When it achieves the maximum generation, the MGPA metamodel will be picked out in terms of high coefficient of determination ($R^2$) and low model complexity [29]. The model complexity is computed as the simple sum of the expressional complexities of its constituent genes and $R^2$ is calculated as below [29]:

$$R^2 = 1 - \frac{\sum\limits_{k=1}^{m} (M_{\text{FEM}}(X_k) - \breve{M}(X_k))^2}{\sum\limits_{k=1}^{m} (M_{\text{FEM}}(X_k) - \frac{1}{m}\sum\limits_{k=1}^{m} M_{\text{FEM}}(X_k))^2} \tag{6}$$

where $M_{\text{FEM}}(X_k)$ is the $k^{th}$ value of the 3D FEM computation result, $\breve{M}(X_k)$ is the predicted $k^{th}$ value on the MGPA metamodel, and $m$ is the number of samples in the training data set. This value ranges from 0 to 1.

The advantage of the MGPA method is to automatically evolve both the structure and the parameters of the mathematical equations based on the training data set.

In this paper, the maximum number of genes is defined as 20, and each gene is limited to a depth of 10.

### C. NUMERICAL RESULTS

Here, the database used to build the metamodels is generated by the Latin hypercube sampling (LHS) method [32], which is consistently more effective than Monte Carlo.

In order to compare the accuracy of different metamodels over the same data set, it can be estimated by the Relative Generalization Error (RGE) between the model-predicted

values and the FEM values:

$$\varepsilon_{\mathrm{RGE}} = \frac{n-1}{n} \frac{\sum_{v=1}^{n} (M_{\mathrm{metamodel}}(X_v) - M_{\mathrm{FEM}}(X_v))^2}{\sum_{v=1}^{n} (M_{\mathrm{FEM}}(X_v) - \frac{1}{n}\sum_{v=1}^{n} M_{\mathrm{FEM}}(X_v))^2} \tag{7}$$

where $n$ is the number of the samples in the data set, $M_{\mathrm{FEM}}(X_v)$ is the $v^{th}$ value of the 3D FEM computation result, $M_{\mathrm{metamodel}}(X_v)$ is the $v^{th}$ predicted value on the metamodel built by the PCE/MGPA method.

After the mutual inductance metamodel is constructed, a test data set, different from the training data set, can be used to validate the predictive performance. The test error can also be calculated by RGE.

To illustrate the procedure, a study case is considered in this paper. The training data set is constituted of 400 samples, and the test data set is constituted of 136 samples, which totally cost 44.7 hours of FEM computation time on an Intel Xeon W-2125 processor. The MGPA method has been executed over ten runs in order to build an accurate metamodel, with a population of 300 models evolving over 150 generations for each run. The time used on the MGPA method takes 311.44 seconds, while the time to elaborate a metamodel on the sparse PCE method takes 2.7 seconds, both run on an Intel(R) Core i5-8365U processor.

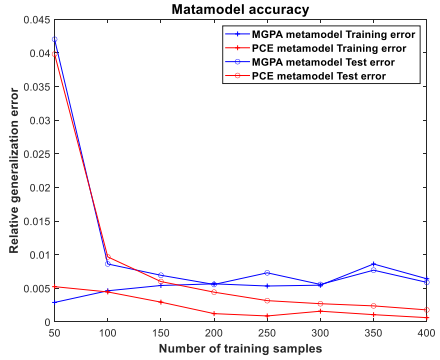


**FIGURE 4.** Comparison of the MGPA and PCE metamodel accuracy.

Fig. 4 shows that the number of training samples will influence the accuracy of the metamodels. The accuracy of the metamodel $\hat{M}$ on the PCE method increases with the number of samples increasing, while the accuracy of the metamodel $\breve{M}$ on the MGPA method did not change a lot. This is because the chosen MGPA metamodel depends on $R^2$ and model complexity, but when increasing the number of training samples, $R^2$ nearly keeps the same value (on the left side of Fig. 5), no matter how the model complexity is (on the right side of Fig. 5). It shows that $R^2$ close to 1 does not guarantee that the MGPA metamodel fits all the samples well [33], [34], [35]. $R^2$ limits the accuracy improvement of the MGPA metamodel even with increasing number of training samples to a great extent in this case. A further possible improvement would be to add another

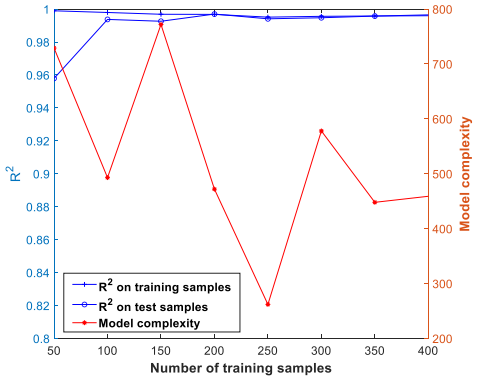


**FIGURE 5.** Relationship between coefficient of determination (model complexity) and number of training samples.

criteria, such as leave-one-out error or RGE on the training samples, in order to build a more accurate MGPA metamodel.

So, the metamodel $\hat{M}$ on the PCE method is chosen to represent the mutual inductance with these eight design variables. Fig.6 reveals that the first-order Sobol index calculated through the metamodel $\hat{M}$ is the same, independently of the number of the training samples. It can be derived that the length and the width of ferrite have more influence on the mutual inductance $M$ compared to other design variables, so in order to get more mutual inductance, the ferrite should be much longer and much wider.

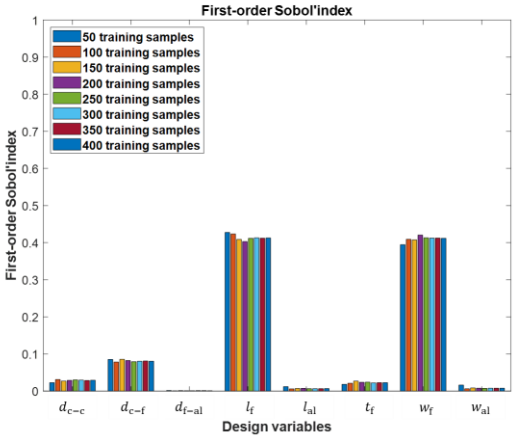


**FIGURE 6.** First-order Sobol index of PCE metamodel.

## IV. OPTIMIZATION PROCESS

The initial structure of the shielding design corresponds to the real case studied and built in GeePs [21], [22], [23]. Generally, in such configurations, as shown in Fig.2, after the initial design, an enhanced, detailed design is normally realized through many additional trials related to simulations and experiments. If using the NSGA-II or MOPSO algorithms directly coupled with COMSOL 3D FEM, new values of the design variables are provided and used in the COMSOL 3D environment for every generation. So, it may cost approximately 2000 hours considering the population size and generation size defined below. But when calculating the mutual inductance with the metamodel, it needs less than 1 second.

Therefore, the proposed approach may save around 50 times the computational time (including the time to calculate the training samples and the test samples). At the same time, it can also save computational resources (the price of the Intel Xeon W-2125 processor is much higher than the Intel(R) Core i5-8365U processor).

Therefore, to reduce the computational time and resources in the case of 3D FEM computations combined with a multiobjective algorithm, it is worth coupling a metamodel on the PCE method with an optimization algorithm for obtaining the optimum design variables on Intel(R) Core i5-8365U processor.

### A. OBJECTIVE FUNCTIONS

Here, the first objective function is the mutual inductance metamodel $\hat{M}$ with design variables, which has to be maximized, referred to (1) for the maximum transmission efficiency. The second objective function is the cost of the shielding, which has to be minimized. The estimation of the shielding cost is described in the following Equation:

$$C = l_{\mathrm{f}} \times w_{\mathrm{f}} \times t_{\mathrm{f}} \times c_{\mathrm{f}} + l_{\mathrm{al}} \times w_{\mathrm{al}} \times c_{\mathrm{al}} \tag{8}$$

where $l_{\mathrm{f}}$, $w_{\mathrm{f}}$, $t_{\mathrm{f}}$, $l_{\mathrm{al}}$ and $w_{\mathrm{al}}$ are the dimensions of the shielding components, as indicated in Fig.2; $c_{\mathrm{f}}$ and $c_{\mathrm{al}}$ are the cost coefficients of ferrite and aluminum, respectively, shown in Table 4 [9].

**TABLE 4. Cost coefficients of ferrite and aluminum.**

| Symbol | Quantity | Value [Unit] |
|---|---|---|
| $c_{\mathrm{f}}$ | Ferrite price | 0.18 [ \$/cm$^3$ ] |
| $c_{\mathrm{al}}$ | Aluminum price | 333.68 [ \$/m$^2$ ] |

### B. MULTIOBJECTIVE OPTIMIZATION

In order to better choose the optimization algorithm for the design of the shielding, two efficient algorithms have been selected and compared: NSGA-II [36], [37] and MOPSO [38], [39]. The optimization settings are listed in Table 5.

During the optimization process, the geometrical conditions and the exposure to electromagnetic fields satisfying practical constraints are taken into account to maximize the mutual inductance with the least cost of the shielding and limit the analysis to only feasible designs. The scheme to handle these constraints in the optimization process is based on references [36], [38]. Here, the first constraint shown in (9) is: that the size of the aluminum should be bigger than the size of the ferrite. In fact, an aluminum plate of the same size as the ferrite plate cannot shield the uncovered area's magnetic field on the surface of the steel plate, which works like the chassis [2], [16]:

$$l_{\mathrm{f}} < l_{\mathrm{al}}, \quad w_{\mathrm{f}} < w_{\mathrm{al}} \tag{9}$$

The other constraint is that the magnetic flux density leakage $B_{\max}$ at the measurement point which is 800 mm far from the center of the air gap should be smaller than 27 $\mu$T (RMS value) defined by ICNIRP guidelines [40], [41], as Fig.7 shows.

**TABLE 5. Optimization settings.**

| Parameter | NSGA-II | Parameter | MOPSO |
|---|---|---|---|
| Population size | 400 | Population size | 400 |
| | | Repository size | 200 |
| Maximum generation | 150 | Maximum generation | 150 |
| Crossover probability | 0.8 | Inertia weight | 0.5 |
| Mutation probability | 0.2 | Personal & Global learning coefficients | 2 |

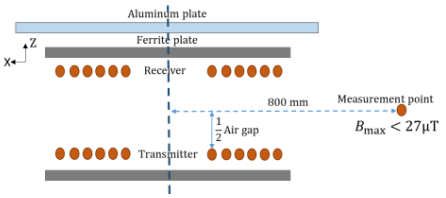


**FIGURE 7. Measurement point of the magnetic flux density leakage.**

### C. RESULTS AND DISCUSSION

In the initial design from Section II, the computed self-inductance $L_1$ of the transmitter is 59.56 $\mu$H, the self-inductance$L_2$ of the receiver is 55.95 $\mu$H, the mutual inductance $M$ between the transmitter and the receiver is 12.29 $\mu$H, the global cost $C$ of ferrite and aluminum shielding is 696.5 \$, and the magnetic flux density leakage $B_{\max}$ at the measuring point is 7.31 $\mu$T.

Here, Fig.8 shows that the mutual inductance increases with the cost of the shielding, and MOPSO can find better solutions than NSGA-II. The magenta value from NSGA-II and the green value from MOPSO are chosen, which satisfies that the size of the aluminum should be bigger than the ferrite, simultaneously the mutual inductance reaches the maximum, and the cost achieves the minimum in the defined ranges of design variables.

The optimization results of NSGA-II and MOPSO are listed in Table 6. Both optimization algorithms converge to find the optimal design variable values. As a consequence of the range of solutions found in Fig.8 and the computational time cost in Table 6, MOPSO will be chosen to design the shielding in the studied IPT system.

**TABLE 6. Optimization results.**

| Parameter | NSGA-II | MOPSO | Parameter | NSGA-II | MOPSO |
|---|---|---|---|---|---|
| $d_{\mathrm{c\text{-}c}}$ [mm] | 1.5 | 1 | $d_{\mathrm{f\text{-}al}}$ [mm] | 8.4 | 20 |
| $w_{\mathrm{f}}$ [mm] | 793 | 940 | $L_1$ [μH] | 75.82 | 80.44 |
| $l_{\mathrm{f}}$ [mm] | 752 | 832 | $L_2$ [μH] | 75.56 | 80.28 |
| $d_{\mathrm{c\text{-}f}}$ [mm] | 1.8 | 1.1 | $M$ [μH] | 22.80 | 25.05 |
| $t_{\mathrm{f}}$ [mm] | 1.4 | 1 | Cost [\$] | 558.8 | 599.6 |
| $w_{\mathrm{al}}$ [mm] | 917 | 1036 | $B_{\max}$ [μT] | 7.76 | 8.57 |
| $l_{\mathrm{al}}$ [mm] | 844 | 920 | Time [s] | 886.5 | 714.3 |

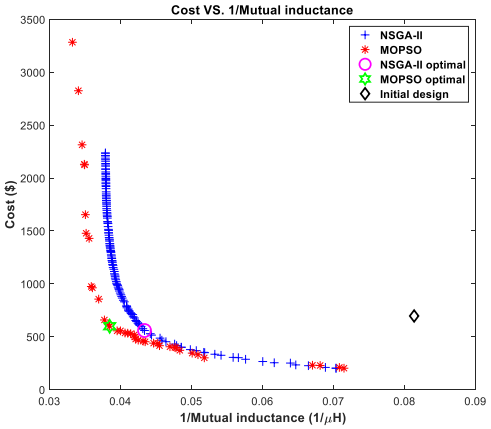


**FIGURE 8.** Cost VS. 1/Mutual inductance.

Compared with the initial design, the optimization procedure of MOPSO improved by approximately 104% the mutual inductance $M$ and saved 14% of the cost $C$of the shielding. However, the magnetic flux density leakage $B_{\max}$ is 8.57 $\mu$T, 1.2 times higher than the initial value, but it still meets the ICNIRP guidelines.

## V. CONCLUSION

Solving a multiobjective optimization based on the PCE metamodeling technique for the design of the IPT system considerably reduces the computational time and computational resources. It comes out from this work that combining a metamodel on the PCE method with MOPSO is proposed to take into account the geometric parameters defining the ferrite and aluminum shielding, thus improving the mutual inductance and reducing the cost of the IPT system under the ICNIRP guidelines. Practical implementation of such shielding is in progress, and experimental validation of the predictions will be presented in a forthcoming paper. Such an optimization approach could be efficiently used for various IPT shielding topologies.

## REFERENCES

[1] S. Jayalath and A. Khan, "Design, challenges, and trends of inductive power transfer couplers for electric vehicles: A review," *IEEE J. Emerg. Sel. Topics Power Electron.*, vol. 9, no. 5, pp. 6196–6218, Oct. 2021, doi: 10.1109/JESTPE.2020.3042625.

[2] J. Li, F. Yin, and L. Wang, "Transmission efficiency of different shielding structures in wireless power transfer systems for electric vehicles," *CSEE J. Power Energy Syst.*, vol. 7, no. 6, pp. 1247–1255, Nov. 2021, doi: 10.17775/CSEEJPES.2019.00500.

[3] T. Campi, S. Cruciani, V. De Santis, F. Maradei, and M. Feliziani, "Magnetic field behavior in a carbon-fiber electrical vehicle charged by a wireless power transfer system," in *Proc. Int. Symp. Electromagn. Compat. (EMC EUROPE)*, Sep. 2017, pp. 1–6, doi: 10.1109/EMCEurope.2017.8094723.

[4] K. Deb, S. Agrawal, A. Pratap, and T. Meyarivan, "A fast elitist non-dominated sorting genetic algorithm for multiobjective optimization: NSGA-II," in *Parallel Problem Solving from Nature PPSN VI* (Lecture Notes in Computer Science), vol. 1917. Berlin, Germany: Springer, 2000, pp. 849–858, doi: 10.1007/3-540-45356-3_83.

[5] C. A. C. Coello and M. S. Lechuga, "MOPSO: A proposal for multiple objective particle swarm optimization," in *Proc. Congr. Evol. Comput. (CEC)*, May 2002, pp. 1051–1056, doi: 10.1109/CEC.2002.1004388.

[6] S. Bandyopadhyay, V. Prasanth, P. Bauer, and J. A. Ferreira, "Multi-objective optimisation of a 1-kW wireless IPT systems for charging of electric vehicles," in *Proc. IEEE Transp. Electrific. Conf. Expo (ITEC)*, Jun. 2016, pp. 1–7, doi: 10.1109/ITEC.2016.7520210.

[7] M. Mohammad, S. Choi, and M. E. Elbuluk, "Loss minimization design of ferrite core in a DD-coil-based high-power wireless charging system for electrical vehicle application," *IEEE Trans. Transport. Electrific.*, vol. 5, no. 4, pp. 957–967, Dec. 2019, doi: 10.1109/TTE.2019.2940878.

[8] R. Bosshard, J. W. Kolar, J. Muehlethaler, I. Stevanovic, B. Wunsch, and F. Canales, "Modeling and $\eta$-$\alpha$ Pareto optimization of inductive power transfer coils for electric vehicles," *IEEE J. Emerg. Sel. Topics Power Electron.*, vol. 3, no. 1, pp. 50–64, Mar. 2015.

[9] A. A. S. Mohamed, S. An, and O. Mohammed, "Coil design optimization of power pad in IPT system for electric vehicle applications," *IEEE Trans. Magn.*, vol. 54, no. 4, pp. 1–5, Apr. 2018, doi: 10.1109/TMAG.2017.2784381.

[10] Z. Luo, X. Wei, M. G. S. Pearce, and G. A. Covic, "Multiobjective optimization of inductive power transfer double-D pads for electric vehicles," *IEEE Trans. Power Electron.*, vol. 36, no. 5, pp. 5135–5146, May 2021, doi: 10.1109/TPEL.2020.3029789.

[11] T. Yilmaz, N. Hasan, R. Zane, and Z. Pantic, "Multi-objective optimization of circular magnetic couplers for wireless power transfer applications," *IEEE Trans. Magn.*, vol. 53, no. 8, pp. 1–12, Aug. 2017, doi: 10.1109/TMAG.2017.2692218.

[12] Y. Li, J. Hu, T. Lin, X. Li, F. Chen, Z. He, and R. Mai, "A new coil structure and its optimization design with constant output voltage and constant output current for electric vehicle dynamic wireless charging," *IEEE Trans. Ind. Informat.*, vol. 15, no. 9, pp. 5244–5256, Sep. 2019, doi: 10.1109/TII.2019.2896358.

[13] M. Lu and K. D. T. Ngo, "Systematic design of coils in series–series inductive power transfer for power transferability and efficiency," *IEEE Trans. Power Electron.*, vol. 33, no. 4, pp. 3333–3345, Apr. 2018, doi: 10.1109/TPEL.2017.2706306.

[14] S. Bandyopadhyay, P. Venugopal, J. Dong, and P. Bauer, "Comparison of magnetic couplers for IPT-based EV charging using multi-objective optimization," *IEEE Trans. Veh. Technol.*, vol. 68, no. 6, pp. 5416–5429, Jun. 2019, doi: 10.1109/TVT.2019.2909566.

[15] H. Zhao, K. Liu, S. Li, F. Yang, S. Cheng, H. H. Eldeeb, J. Kang, and G. Xu, "Shielding optimization of IPT system based on genetic algorithm for efficiency promotion in EV wireless charging applications," *IEEE Trans. Ind. Appl.*, vol. 58, no. 1, pp. 1190–1200, Jan. 2022, doi: 10.1109/TIA.2021.3121353.

[16] R. Tavakoli, E. M. Dede, C. Chou, and Z. Pantic, "Cost-efficiency optimization of ground assemblies for dynamic wireless charging of electric vehicles," *IEEE Trans. Transport. Electrific.*, vol. 8, no. 1, pp. 734–751, Mar. 2022, doi: 10.1109/TTE.2021.3105573.

[17] G. Di Capua, N. Femia, K. Stoyka, G. Di Mambro, A. Maffucci, S. Ventre, and F. Villone, "Mutual inductance behavioral modeling for wireless power transfer system coils," *IEEE Trans. Ind. Electron.*, vol. 68, no. 3, pp. 2196–2206, Mar. 2021, doi: 10.1109/TIE.2019.2962432.

[18] A. Delgado, G. Di Capua, K. Stoyka, L. Shi, N. Femia, A. Maffucci, S. Ventre, P. Alou, J. A. Oliver, and J. A. Cobos, "Self and mutual inductance behavioral modeling of square-shaped IPT coils with air gap and ferrite core plates," *IEEE Access*, vol. 10, pp. 7476–7488, 2022, doi: 10.1109/ACCESS.2021.3138239.

[19] G. Di Capua, A. Maffucci, K. Stoyka, G. Di Mambro, S. Ventre, V. Cirimele, F. Freschi, F. Villone, and N. Femia, "Analysis of dynamic wireless power transfer systems based on behavioral modeling of mutual inductance," *Sustainability*, vol. 13, no. 5, p. 2556, Feb. 2021.

[20] Y. Pei, Y. Le Bihan, M. Bensetti, and L. Pichon, "Comparison of coupling coils for static inductive power-transfer systems taking into account sources of uncertainty," *Sustainability*, vol. 13, no. 11, p. 6324, Jun. 2021, doi: 10.3390/su13116324.

[21] Y. Pei, L. Pichon, M. Bensetti, and Y. Le-Bihan, "Uncertainty quantification in the design of wireless power transfer systems," *Open Phys.*, vol. 18, no. 1, p. 391, Jul. 2020, doi: 10.1515/phys-2020-0174.

[22] K. Kadem, "Modeling and optimization of a magnetic coupler for dynamic induction charging of electric vehicles," Ph.D. thesis, Centralesupelec, Universite Paris-Saclay, Gif-sur-Yvette, France, 2020. Accessed: Aug. 29, 2022. [Online]. Available: https://hal.archives-ouvertes.fr/tel-03253967

[23] K. Kadem, M. Bensetti, Y. Le Bihan, E. Labouré, and M. Debbou, "Optimal coupler topology for dynamic wireless power transfer for electric vehicle," *Energies*, vol. 14, no. 13, p. 3983, Jul. 2021, doi: 10.3390/en14133983.

[24] J. Sallan, J. L. Villa, A. Llombart, and J. F. Sanz, "Optimal design of ICPT systems applied to electric vehicle battery charge," *IEEE Trans. Ind. Electron.*, vol. 56, no. 6, pp. 2140–2149, Jun. 2009, doi: 10.1109/TIE.2009.2015359.

[25] E. ElGhanam, M. Hassan, A. Osman, and H. Kabalan, "Design and performance analysis of misalignment tolerant charging coils for wireless electric vehicle charging systems," *World Electr. Vehicle J.*, vol. 12, no. 3, p. 89, Jun. 2021, doi: 10.3390/wevj12030089.
[26] COMSOL. *Software for Simulating Static and Low-Frequency Electromagnetics*. Accessed: Jan. 29, 2022. [Online]. Available: https://www.comsol.com/acdc-module
[27] S. Cruciani, T. Campi, F. Maradei, and M. Feliziani, "Conductive layer modeling by improved second-order artificial material single-layer method," *IEEE Trans. Antennas Propag.*, vol. 66, no. 10, pp. 5646–5650, Oct. 2018, doi: 10.1109/TAP.2018.2854413.
[28] UQLab. *Polynomial Chaos Expansions (PCE) | User Manuals*. Accessed: Jan. 29, 2022. [Online]. Available: https://www.uqlab.com/pce-user-manual
[29] D. P. Searson, "GPTIPS 2: An open-source software platform for symbolic data mining," in *Handbook of Genetic Programming Applications*, A. H. Gandomi, A. H. Alavi, and C. Ryan, Eds. Cham, Switzerland: Springer, 2015, pp. 551–573, doi: 10.1007/978-3-319-20883-1_22.
[30] B. Efron, T. Hastie, I. Johnstone, and R. Tibshirani, "Least angle regression," *Ann. Statist.*, vol. 32, no. 2, pp. 407–499, Apr. 2004, doi: 10.1214/009053604000000067.
[31] UQLab. *Sensitivity Analysis | User Manuals*. Accessed: Sep. 9, 2021. [Online]. Available: https://www.uqlab.com/sensitivity-user-manual
[32] J. C. Helton and F. J. Davis, "Latin hypercube sampling and the propagation of uncertainty in analyses of complex systems," *Rel. Eng. Syst. Saf.*, vol. 1, no. 81, pp. 23–69, 2003, doi: 10.1016/S0951-8320(03)00058-9.
[33] T. O. K. Lseth, "Note on the $R^2$ measure of goodness of fit for nonlinear models," *Bull. Psychonomic Soc.*, vol. 21, no. 1, pp. 79–80, Jan. 1983. [Online]. Available: https://doi-org.ezproxy.universite-paris-saclay.fr/10.3758/BF03329960
[34] A.-N. Spiess and N. Neumeyer, "An evaluation of $R^2$ as an inadequate measure for nonlinear models in pharmacological and biochemical research: A Monte Carlo approach," *BMC Pharmacol.*, vol. 10, no. 1, Jun. 2010, doi: 10.1186/1471-2210-10-6.
[35] J. Frost. (Apr. 10, 2017). *R-Squared is Not Valid for Nonlinear Regression, Statistics By Jim*. Accessed: Aug. 10, 2022. [Online]. Available: http://statisticsbyjim.com/regression/r-squared-invalid-nonlinear-regression/
[36] D. Kalyanmoy, *Multi-Objective Optimization Using Evolutionary Algorithms*. Chichester, U.K.: Wiley, 2001.
[37] *Gamultiobj Algorithm—MATLAB & Simulink*. [Online]. Available: https://www.mathworks.com/help/gads/gamultiobj-algorithm.html?searchHighlight=gamultiobj&s_tid=srchtitle_gamultiobj_2
[38] C. A. C. Coello, G. T. Pulido, and M. S. Lechuga, "Handling multiple objectives with particle swarm optimization," *IEEE Trans. Evol. Comput.*, vol. 8, no. 3, pp. 256–279, Jun. 2004, doi: 10.1109/TEVC.2004.826067.
[39] V. Martinez-Cagigal. *Multi-Objective Particle Swarm Optimization (MOPSO)*. Accessed: Aug. 29, 2022. [Online]. Available: https://www.mathworks.com/matlabcentral/fileexchange/62074-multi-objective-particle-swarm-optimization-mopso
[40] International Commission on Non-Ionizing Radiation Protection, "Guidelines for limiting exposure to electromagnetic fields (1 Hz to 100 kHz)," *Health Phys.*, vol. 118, no. 5, pp. 818–836, 2020, doi: 10.1097/HP.0000000000001210.
[41] *Wireless Power Transfer for Light-Duty Plug-in/Electric Vehicles and Alignment Methodology*, Standard J2954_202010, SAE International. Accessed: Mar. 26, 2021. [Online]. Available: https://www.sae.org/standards/content/j2954_202010/

**YAO PEI** was born in Zhejiang, China, in 1994. She received the master's (Diploma) degree from the Universite de Nantes, Nantes, France, in 2019. She is currently pursuing the Ph.D. degree with Universite Paris-Saclay, Paris, France.

In 2019, she joined the Group of Electrical Engineering in Paris (GeePs). During her Ph.D. study, she has authored several papers in the international journals. Her current research interests include wireless power transfer systems, electromagnetic compatibility, machine learning, and uncertainty analysis.

**LIONEL PICHON** received the Diploma (Engineering) degree from the Ecole Supérieure d'Ingénieurs en Electronique et Electrotechnique, in 1984, and the Ph.D. degree in electrical engineering from the Laboratoire de Génie Electrique de Paris, in 1989.

He got a position at the Centre National de la Recherche Scientifique (CNRS), in 1989. He is currently the Directeur de Recherche (a Senior Research Scientist) with the Group of electrical engineering-Paris (GeePs), a laboratory belonging to four institutions, such as the CNRS, CentraleSupélec, Université Paris-Saclay, and Sorbonne Université. He is the author or coauthor of more than 120 journal articles in peer-reviewed journals. His research interests include computational electromagnetics for wave propagation, scattering, and electromagnetic compatibility. He is serving as a reviewer for several scientific international journals. He is an Associated Editor of the *European Physical Journal-Applied Physics* (EPJ-AP).

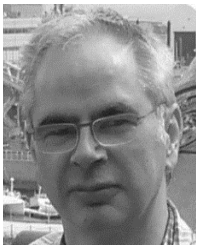

**YANN LE BIHAN** received the Engineering degree in electrical engineering and the Ph.D. degree in electronics from the ENS de Cachan, Cachan, France, in 1996 and 2000, respectively, and the Ph.D. (H.D.R.) degree (Enabling) from Universitìe Paris-Sud, Paris, France, in 2007.

From 2001 to 2011, he was an Assistant Professor with the IUT de Cachan, Cachan, and Universitìe Paris-Sud, where he has been a Professor, since 2011. In 2000, he joined the Laboratoire de Gìenie Electrique de Paris, which became the Group of Electrical Engineering of Paris, Paris, in 2015. His research interests include characterization and nondestructive testing by electromagnetic methods, such as modeling, sensor design, and inverse problems.

**MOHAMED BENSETTI** received the master's (D.E.A.) and Ph.D. degrees in electrical engineering and the Habilitation à Diriger des Recherches degree from the University of Paris-Sud, France, in 2001, 2004, and March 2014, respectively. From 2005 to 2007, he worked as a Researcher with the Ecole Supérieure d'Electricité (SUPELEC)—Gif sur Yvette, France. In 2007, he joined the Ecole Supérieure d'Ingénieur en Génie Electrique (ESIGELEC), Rouen, where he was a Lecturer and a Researcher with the Research Institute for Electronic Embedded Systems (IRSEEM). In January 2013, he joined the Energy Department of SUPELEC. He is currently a Professor at CentraleSupelec. He is also with the Group of electrical engineering, Paris (GeePs). His current research interests include electromagnetic modeling, electromagnetic compatibility (EMC) and power electronics, including modeling, simulation, and instrumentation.

**PHILIPPE DESSANTE** received the degree in applied mathematics from the University of Montpellier, the degree in physics from the University of Versailles, France, and the Ph.D. degree from the Laboratoire de Physique des Gaz et des Plasmas, Paris Sud University, Orsay, France, in 2000.

He is currently an Associate Professor at CentraleSupelec, Rennes, France. His current research interests include the simulation and optimization of electro-technical systems.